Atmospheric Environment 118 (2015) 194–202

Contents lists available at ScienceDirect

Atmospheric Environment

journal homepage: www.elsevier.com/locate/atmosenv

Real-time and single-particle volatility of elemental carbon-containing particles in the urban area of Pearl River Delta region, China

Xinhui Bi [a, *], Shouhui Dai [a], Guohua Zhang [a], Ning Qiu [b], Mei Li [c], Xinming Wang [a], Duohong Chen [d], Ping'an Peng [a], Guoying Sheng [a], Jiamo Fu [a], Zhen Zhou [c]

[a] State Key Laboratory of Organic Geochemistry and Guangdong Key Laboratory of Environmental Resources Utilization and Protection, Guangzhou Institute of Geochemistry, Chinese Academy of Sciences, Guangzhou, 510640, PR China
[b] South China Sea Institute of Oceanology, Chinese Academy of Sciences, Guangzhou, 510301, PR China
[c] Atmospheric Environment Institute of Safety and Pollution Control, Jinan University, Guangzhou, 510632, PR China
[d] State Environmental Protection Key Laboratory of Regional Air Quality Monitoring, Guangdong Environmental Monitoring Center, Guangzhou, 510308, PR China

HIGHLIGHTS

- We measure the real-time single volatility of EC-containing particles.
- The sulfate and organics in the ECOC type showed low volatility.
- The volatilities of secondary ions were dependent on their molecular forms.
- The volatility of EC-containing particles decreased during the hazy days.

ARTICLE INFO

Article history:
Received 17 March 2015
Received in revised form
1 August 2015
Accepted 4 August 2015
Available online 7 August 2015

Keywords:
Volatility
EC particles
Single particle
Mixing state
Atmospheric aging
PRD region

ABSTRACT

Elemental carbon (EC) aerosol represents an important fraction of aerosol particles in urban area of the Pearl River Delta (PRD) region, China. Previous studies have demonstrated that EC particles in the PRD region undergo significant amounts of aging processes. To assess the degree of aging, the real-time single particle volatility of EC-containing particles was measured in an urban area of the PRD region by a thermodiluter coupled to a single particle aerosol mass spectrometer (SPAMS). The size and chemical composition of the individual particles before and after heating to 75 °C, 150 °C and 300 °C were characterized. Of the total unheated particles examined by SPAMS, 53% of the unheated particles contained EC, and a higher number fraction (69%) was observed in the particles heated to 300 °C. No significant differences in the mass spectral patterns were found between ambient temperature and 75 °C. Nitrate evaporated at 150 °C, and most of sulfate evaporated at 300 °C. EC-containing particles were clustered into four distinct particle types based on the dominant chemical species present in the mass spectra, comprised of EC, internally mixed EC and organic carbon (OC) (ECOC), internally mixed EC and sodium/potassium salt (NaK–EC), and internally mixed EC and metal species (Metal–EC). Detail analysis show that the volatility of EC-containing particles relied on the EC particle types. Among the four types, the EC type was quite volatile. A significant fraction of sulfate and organics in the ECOC type did not volatilize at 300 °C. The volatilities of secondary ions in the four EC-containing particle types were found to be dependent on their molecular composition. Additionally, the volatility of EC-containing particles decreased during the polluted hazy days due to the generation of low volatile compounds under the atmospheric conditions with higher precursor concentrations and oxidation capacity. To our knowledge, this is the first reported real-time volatility measurements of individual ambient aerosols in the PRD region. These findings provide an improved understanding of the aging process of EC particles, and may help in the modeling of its climate impact.

* Corresponding author.
E-mail address: bixh@gig.ac.cn (X. Bi).

http://dx.doi.org/10.1016/j.atmosenv.2015.08.012
1352-2310/

1. Introduction

Airborne particles adversely affect air quality and public health, and they also exert profound impacts on global radiation budget and hydrological cycle (Heal et al., 2012; Ramanathan et al., 2001). The degree of aerosol impacts depends on their physical and chemical composition and mixing state. Volatility is an important physical property, which is linked to the chemical properties and mixing state of the aerosol particles (Huffman et al., 2008). The volatility of aerosol particles determines the likelihood that a compound will exist in the gaseous or particulate phase, and thus strongly influences the formation and aging of secondary aerosols (Donahue et al., 2012; Kolb and Worsnop, 2012). Moreover, the volatile species have a significant influence on light scattering and absorption (Clarke et al., 2004). Therefore, an accurate understanding of particle volatility is imperative and has great atmospheric significance. The fine particulate matter in the atmosphere ranges widely in volatility (Hallquist et al., 2009; Jimenez et al., 2009; Robinson et al., 2007). Fresh particles are expected to contain a higher fraction of low volatility compounds, while older particles may contain higher volatility species (Chhabra et al., 2011). However, the volatilities of different aerosol types remain poorly understood at present.

Atmospheric particles contain a wide range of compounds. Carbonaceous aerosol is a major fraction of submicron particles, and contributes to ~36% of light extinction in the Pearl River Delta (PRD) region, China (Wang et al., 2012; Zhang et al., 2013a). Elemental carbon (EC) is a distinct type of carbonaceous particles. It can absorb solar radiation, and is second only to CO_2 in terms of global warming potential (Ramanathan and Carmichael, 2008); and hence plays a unique role in the climate system. EC is generated exclusively by incomplete combustion of fossil fuel and biomass (Ramanathan and Carmichael, 2008; Bond et al., 2013). Studies suggest that EC particles tend to become internally mixed with inorganic and organic components via condensation, coagulation, heterogeneous reactions and cloud processing in the atmospheric aging processes (Bond et al., 2013). Many studies have demonstrated that optical properties of EC are sensitive to their physical (e.g., size and morphology) and chemical properties (e.g., composition, mixing state) (Moffet and Prather, 2009). Thus, the aging degree should be assessed so as to improve our understanding on its climate impact.

The thermodenuder is a tool that can be used to unravel some aspects of volatility, and it has been applied in a number of laboratory and field studies (Huffman et al., 2008; Kim and Paulson, 2013; Kostenidou et al., 2009). In a typical thermodenuder, aerosols are heated at a fixed temperature for a specific period of time, evaporating the volatile compounds from the particles. The remaining compounds after heating would be composed of non-volatile materials, such as EC, crustal material, sea salt, and so on (Levy et al., 2014), which are regarded as the particle cores. The particle volatility data is obtained by a comparison of the chemistry of the unheated aged particles with the heated particle residues (Pratt and Prather, 2009). Additionally, Pratt and Prather (2009) found that particles after exposure to a temperature of 230 °C possesses signatures similar to those fresh emission sources, indicating that particle volatility study can be used to apportion the original sources of particles in highly aged environment. In this study, a temperature-stepping thermodiluter was coupled to a single particle aerosol mass spectrometer (SPAMS) to directly measure the individual EC-containing particle size and chemically resolved volatility. SPAMS was used for characterizing the chemical mixing state of ambient and heated particles (Bi et al., 2011; Zhang et al., 2013b). Additionally, the potential sources were discussed based on the chemistry of heated particles.

2. Methods

A recently developed thermodiluter (Dai et al., 2014) was placed upstream of SPAMS for volatility study. The thermodiluter consists of a 50-cm long, 2.5-cm OD stainless steel tube heated with a 3-zone temperature controller through which the sample air flows (Dekati Ltd), leading to evaporation of some of the particle mass, and a diluter following the heating section to cool and dilute the vapors and prevent recondensation of evaporated materials. The thermodiluter-SPAMS system can measure from ambient temperature to 350 °C. Detailed descriptions of both thermodiluter characterization and operation are available in the Supplementary material (SM). In this study, air was sampled through a $PM_{2.5}$ cyclone and then through the thermodiluter or 1/4 inch bypass line. All data shown here were corrected by dilution ratio. A drier was not utilized in this study. The particles, sampled by the SPAMS (either heated or unheated), were controlled by a valve, which manually switched between heated and unheated ambient particles.

The unheated and heated particles were analyzed by SPAMS to get the information on size and mass spectra. The detail principle of SPAMS had been described elsewhere (Li et al., 2011). Briefly, particles are introduced into vacuum pumped SPAMS through a 0.1 mm critical orifice at a flow of 80 mL min^{-1}. They are then focused and accelerated to specific velocities characteristic of their aerodynamic diameter while passing through the aerodynamic lens following the sizing region, where velocities of individual particles are determined by two continuous diode Nd:YAG laser beams operated at 532 nm. The particles are subsequently desorped/ionized by a 266 nm Nd:YAG laser which is triggered exactly based on the velocity of the specific particle measured in the sizing chamber. Positive and negative fragments generated are then detected by a dual-polarity time-of-flight mass spectrometer. Peak identifications within this paper correspond to the most probable assignments for each particular mass/charge (m/z) ratio and details can be referred to previous work (Liu et al., 2003; Murphy and Thomson, 1997a,b). An adaptive resonance theory based neural network algorithm (ART-2a) was utilized to classify individual particles into separate clusters based on the presence and intensity of ion peaks in individual single particle mass spectra (Song et al., 1999) with a vigilance factor of 0.7, learning rate of 0.05, and 20 iterations. First 300, 150 and 120 clusters at ambient temperature, 150 °C and 300 °C respectively dominated the initially generated clusters, representing more than 92% of all the analyzed particles, were manually merged based on the spectral similarities. Particle classes were defined by characteristic chemical species in the mass spectra.

The thermodiluter-SPAMS measurements were conducted in the building roof of Guangzhou Institute of Geochemistry, Chinese Academy of Sciences from February 28 to March 9, 2013. The heated portion of the thermodiluter and valve program was: ambient (10 min), 75 °C (40 min), ambient (10 min), 150 °C (20 min), ambient (10 min), 300 °C (40 min), ambient (10 min), 150 °C (20 min). One full cycle took 160 min before repeating. Totally, 2 066 411, 234 746, 125 099 and 29 818 particles were obtained under ambient, 75 °C, 150 °C and 300 °C, respectively.

Due to the detection efficiency of chemical species depending on the chemical components present in the particle (the matrix), the obtained mass spectral ion intensities may vary from particle to particle. However, several studies have shown that one can apply

the relative peak intensities to account for different ion intensities commonly observed among different particle types and laser absorption or ablation/ionization efficiency (e.g., Hatch et al., 2014; Jeong et al., 2011). To compare the difference between heated and ambient particles, a reference component is used to normalize all the peak intensities in a mass spectrum, and this approach is similar to that developed by Hatch et al. (2014).

3. Results and discussion

3.1. General characteristics

From February 28 to March 9, an hourly average $PM_{2.5}$ mass concentration of 69 μg m^{-3} was observed with build-up and stagnation period leading to a maximum of 163 μg m^{-3}. Information on the variations of $PM_{2.5}$, NO_x, O_3, SO_2 and meteorological parameters (visibility, wind speed, relative humidity (RH) and temperature) throughout the sampling period can be found in Fig. S5 of SM. Ambient temperature and RH during this study generally varied between 11–28 °C and 17–89%, with an average of 19 °C and 55%. From March 5–9, lower wind speeds led to more stagnant condition. During this period, the highest ozone and NO_x concentrations were up to 326 μg m^{-3} (65 μg m^{-3} on average) and 558 μg m^{-3} (148 μg m^{-3} on average), respectively.

The average mass spectra of unheated and heated particles are shown in Fig. S6. The vast majority (>80%) of unheated particles contained sulfate and nitrate, indicating that they experienced aging processes during transport. Of the total unheated particles examined by SPAMS in this study, 53% of unheated particles contained EC, and a higher number fraction (69%) was in the particles heated to 300 °C. EC-containing particles are identified by the intense ion signals from EC cluster ions (e.g., m/z ±12$[C]^{+/-}$, ±36$[C_3]^{+/-}$, ±48$[C_4]^{+/-}$ and ±60$[C_5]^{+/-}$). The individual unheated and heated particles with both positive and negative ion spectra were classified into eight particle types. The characteristic of non-EC-containing particle types is depicted in SM, and their corresponding mass spectra (Fig. S7) and particle numbers (Table S1) are also shown therein. Four EC-containing particle types were obtained: (1) Internally mixed EC and organic carbon (OC) (ECOC) type, accounting for 21.1% by number of all the unheated EC-containing particles. The positive ion mass spectral signature of the ECOC particle type showed organic fragments (with the most likely peak identifications in parentheses) at m/z 27$[C_2H_3^+]$, 37$[C_3H^+]$, and 51$[C_4H_3^+]$ with contributions from EC markers, $C_n^{+/-}$ (n = 1–6). (2) EC type. Mass spectra of EC type were dominated by the distinct EC cluster ions ranged from m/z −60 to m/z 60 with really low intensity of organic fragments, which was the most abundant type comprising 39.6% by number of all the unheated EC-containing particles. (3) Internally mixed EC and sodium/potassium salt (NaK–EC) type, mainly associated with nitrate. It comprised 31.1% by number of the unheated EC-containing particles. NaK–EC type showed the carbon cluster ions mainly in the negative mass spectra, combined with dominant peaks from 23$[Na]^+$ to 39$[K]^+$ in the positive ones. (4) Internally mixed EC and metal species (Metal–EC) type, mainly associated with nitrate and chloride. It contributed 8.2% by number to the unheated EC-containing particles. The most abundant metallic species were 56$[Fe]^+$, 63$[Cu]^+$ and 206–208$[Pb]^+$. The EC-containing particles were found to be extensively internally mixed with detectable sulfate (85.4%), nitrate (96.6%), oxidized organics (29.8%), and/or ammonium (36.6%) (Fig. 1), indicative of the aging state of the EC-containing particles. Mass spectral signatures of ECOC, EC, NaK–EC and Metal–EC types at ambient temperature and 300 °C are shown in Fig. 2. It can be seen that there is an occurrence of very intense 39$[K]^+$ ion peak associated with ion peaks due to −26$[CN]^-$ and −42$[CNO]^-$ in the heated particles indicating the contribution of biomass/biofuel burning (Bi et al., 2011; Pratt et al., 2011; Silva et al., 1999).

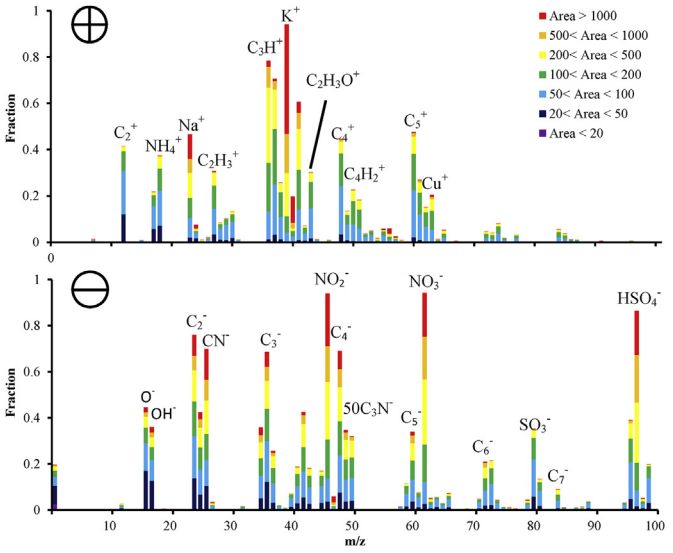

Fig. 1. Average digitized positive (upper) and negative (bottom) ions mass spectrum of the unheated EC-containing particles analyzed over the spring period.

3.2. Chemically resolved volatility of EC-containing particles

The sized number normalized by dilution ratio decreased appreciably with heating by 9% at 75 °C to 88% at 300 °C. This decrease likely occurred due to the evaporation of secondary species and subsequent reduction of their transmission efficiencies. The number of size-resolved particles is shown in Fig. 3 for each temperature. It is clear that the size distribution of particles shifted towards smaller particles with heating from ambient temperature up to 300 °C, suggesting that the secondary species directly contributed to the particles growth.

Volatility could provide insight into the contribution of different forms of secondary species with respect to individual particle cores (Pratt and Prather, 2009; Huffman et al., 2009). No significant differences were found between ambient temperature and 75 °C (Fig. S6). At 150 °C, nitrate (m/z −62, NO_3^-, m/z −46, NO_2^-) was found being evaporated. Most of sulfate (m/z −97, HSO_4^-) evaporated at 300 °C. Generally, heating to 150 °C is designed to drive off low-temperature volatiles, while heating to 300 °C is designed to evaporate medium-temperature volatiles such as ammonium sulfate (Engler et al., 2007). Here we focused on the 300 °C heated particles to unravel the volatility of secondary species. Because strongly absorbing EC core is exposed after heating as the particle coating is stripped away, the ionization efficiency is enhanced (Hatch et al., 2014). In order to eliminate this bias, we used the reference method to normalize the peak area of the EC-containing particles. m/z 36 (C_3^+) is used in the study of Hatch et al. (2014) as the reference. However, we used potassium m/z 39 (K^+) as the reference because the carbon cluster peaks were observed to be more prominent in the negative mass spectra with heating, and K^+ represented component that is non-volatile at the preset temperatures and was also the predominant peak in the mass spectrum of each particle type. Difference plots of the normalized absolute mass spectra at 300 °C minus that for unheated ECOC, EC, NaK–EC and Metal–EC are shown in Fig. 4. It is clear that the absolute peak areas of sulfate and nitrate decreased a lot after heating and the intensity of CN^- (m/z −26), CNO^- (m/z −42) and Ca^+ (m/z 40) increased at 300 °C. The CN^- and CNO^- signals were previously attributed to

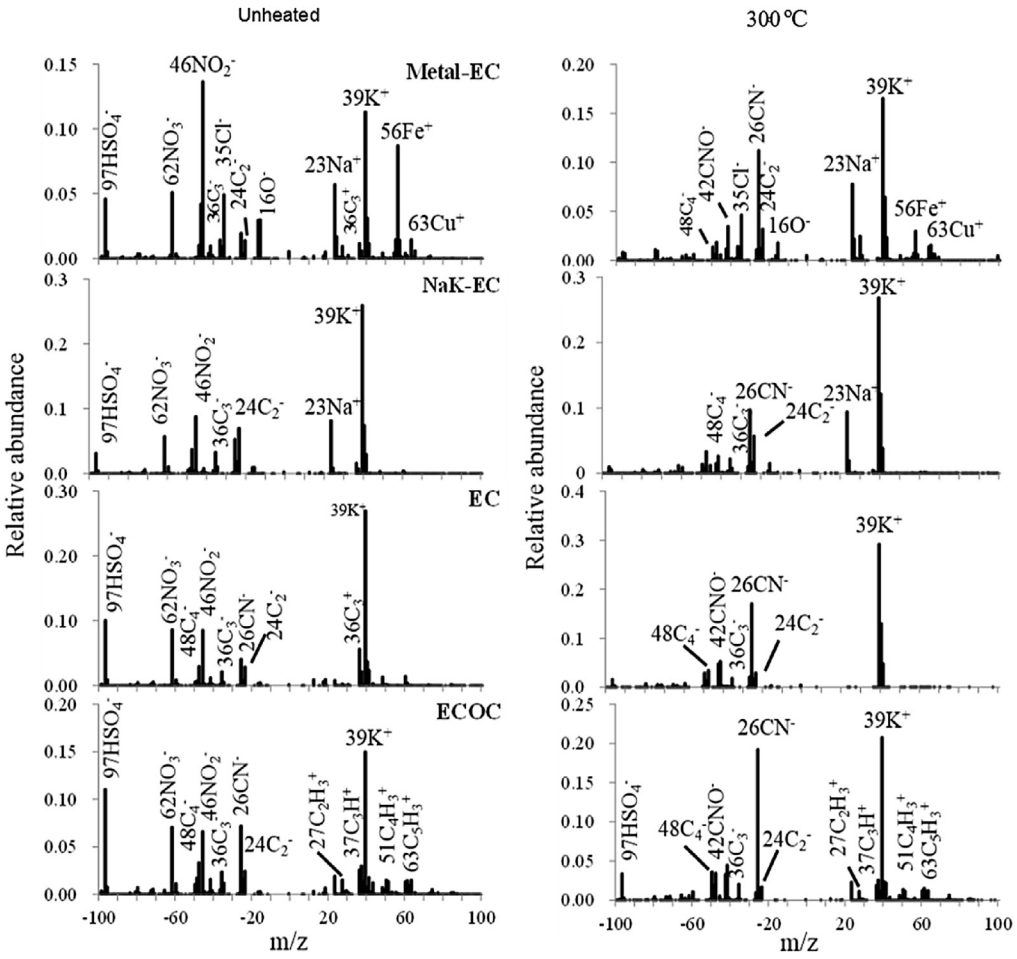

Fig. 2. Average SPAMS mass spectra of unheated and 300 °C heated particles for EC-containing particle types.

nitrogen-containing organics and associated with high mass organics (Wang et al., 2010; Yadav et al., 2004). Therefore, the increase of CN^- signals may indicate that the corresponding species is less volatile than other species, such as ammonium nitrate/sulfate. Additionally, the CN^- and CNO^- ions generated from particles possibly increased following heating through changes in ionization efficiency and/or extent of particle ablation, resulting in stronger ion peaks measured by SPAMS. The contribution of nitrate was much more than that of sulfate to the volatility of unheated Metal–EC and NaK–EC types. On the contrary, sulfate contributed more or similar to the volatility of EC and ECOC particles compared to nitrate. The vaporization temperature ranges of ammonium nitrate and ammonium sulfate are 48–89 °C (Johnson et al., 2004a) and 178–205 °C (Johnson et al., 2004b). The decrease in nitrate and sulfate peak areas is correlated with the decrease in ammonium from ambient to 300 °C, indicating their loss in the form of ammonium salt. Different from the inorganic secondary ions, the organic carbon retained at 300 °C, as shown in Fig. 2, indicating the non-volatility of organic species associated with the ECOC particles. The loss of Fe^+ (m/z 56) for the Metal–EC particles at 300 °C needs further investigation.

To assess the impacts of single particle mixing state on volatility,

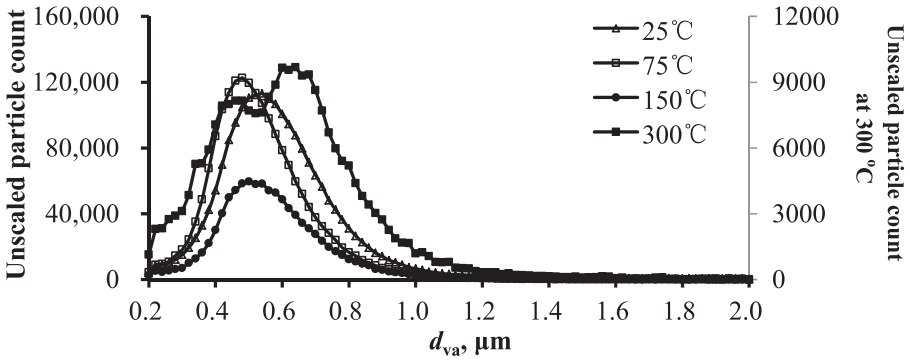

Fig. 3. Unscaled particle counts detected by SPAMS at each temperature.

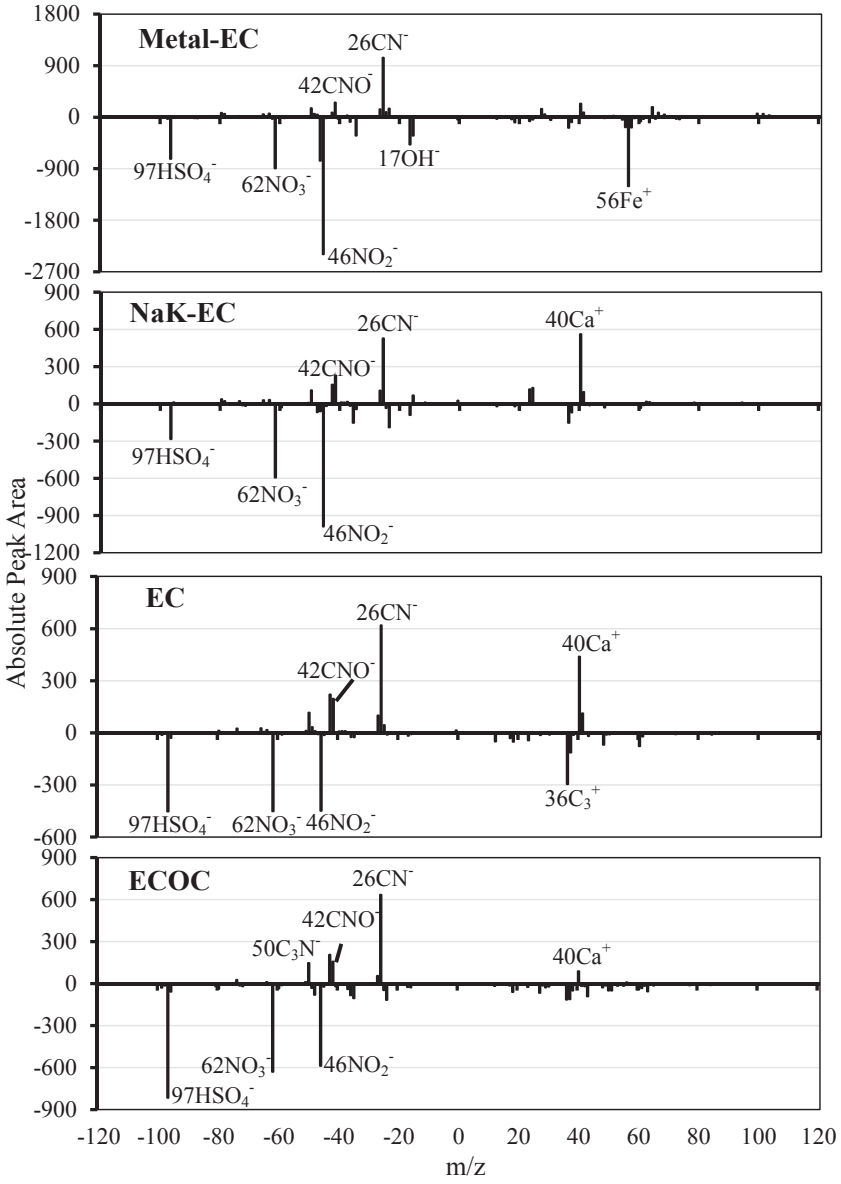

Fig. 4. Mass spectral subtraction plot of the average mass spectrum corresponding to each EC-containing particles type at 300 °C minus unheated particles. Positive intensity peaks correspond to higher abundance in the 300 °C particles, whereas negative intensity peaks show higher intensity in the unheated particles.

the volatility of secondary species on the four EC-containing particles were examined. Through comparison of the relative peak area of ion markers remaining at ambient temperature and 300 °C (Fig. 4 and Fig. S8), the volatility and the molecular forms of secondary species on different particle types may be assessed. Nitrate was found to be primarily in the form of ammonium nitrate for the EC-containing particle types except NaK–EC particles. Nearly 20% of the nitrate was present in nonvolatile forms, such as KNO_3 and $NaNO_3$ in the NaK–EC particles (Fig. S8). Sulfate evaporated a lot (>85%) for Metal–EC and EC particles, suggesting sulfate are in the forms of ammonium sulfate. However, a significant fraction of the sulfate in the ECOC and NaK–EC types did not volatilize at 300 °C. Sulfate remaining at 300 °C is hypothesized to be in the forms of K_2SO_4, Na_2SO_4 and organosulfates (Andreae and Gelencser, 2006; Engler et al., 2007; Knudsen et al., 2004; Romero and Oehme, 2005), which can only be thermally volatilized above 400 °C.

3.3. Volatility during the hazy episode

During the sampling period, a hazy air pollution episode was identified on March 5–9th, with high O_3 (104.0 μg/m^3 on average), NOx (201.1 μg/m^3), $PM_{2.5}$ (92.5 μg/m^3) and low visibility (8.4 km). For the other unpolluted days, the average concentrations of O_3, NOx and $PM_{2.5}$ decreased 50.1%, 75.2% and 67.5%, respectively. Correspondingly, the visibility on average increased to 14.4 km. Weather condition was also different between unpolluted and hazy days. The polluted hazy days showed higher temperature (21.2 °C) and lower RH (45.5%) levels than the unpolluted days (14.3 °C, 50.6%).

Secondary precursors and photochemical activity appear to collectively play a role in secondary aerosol formation during atmospheric aging processes (Denkenberger et al., 2007; Hallquist et al., 2009). Relatively high atmospheric oxidizing capacity and low relative humidity during hazy days could result in different

volatility of EC-containing particle types when compared to the unpolluted days. Fig. 5 presents the variations of fraction remaining of selected markers in the mass spectrum corresponding to each EC-containing particles type during the hazy and unpolluted days. The m/z 43[C_2H_3O]$^+$ is commonly attributed to the oxidized organics that are formed through photochemical processing (Qin et al., 2012). It is observed that decreased volatility of secondary species in the ambient particles generally occurred during the hazy days except sulfate associated with Metal–EC particles. The different volatility of EC particle types on the unpolluted and hazy days can be attributed to the formation mechanisms of secondary species. Under higher relative humidity and lower temperature conditions during the unpolluted days, wetter particles are able to capture more soluble gases such as ammonia, nitric acid, SO_2 and NOx, thus leading to the more efficient production of ammonium sulfate and nitrate (Ge et al., 2012). Studies have reported that wet surface are also favorable for the uptake of semi-volatile water soluble species (e.g., ammonium, nitrate and organics) (Seinfeld and Pandis, 2006), which are consistent with the higher volatility of secondary species on the unpolluted days with lower temperature and higher RH. However, the significant increase in NOx and O_3 during the hazy days could result in the enhanced production of secondary organic aerosol (SOA). By combining thermodenuder and aerosol mass spectrometry (AMS) measurements, previous studies have showed that the relative humidity, OH scavenger, NOx concentration and temperature influenced on the volatility of SOA (Jonsson et al., 2007; Lee et al., 2011). The level of NOx has been found to be highly influential on SOA formation from a variety of precursor compounds (Ng et al., 2007). VOC degradation at high-NOx levels tends to generate a product distribution that is dominated by carbonyls, hydroxycarbonyls, organic nitrates and peroxyacyl nitrate (Hallquist et al., 2009; Kroll and Seinfeld, 2008). In the PRD region, He et al. (2014) detected higher concentrations of organosulfates and nitrooxy organosulfates at high NOx season than low NOx season (He et al., 2014). They also pointed out that the formation of organosulfates and nitrooxy organosulfates was likely driven by photochemistry over the PRD region. Therefore, the significant decreased volatility of oxidized organics in the ECOC particles during hazy days can also be explained by the generation of organic sulfate and nitrate.

3.4. Particle chemistry at 300 °C

The relative contributions of the four EC-containing types with respect to size are shown in Fig. 6. The EC type was the most abundant unheated EC-containing particles type; the relative contribution of these particles decreased with heating, particularly for the larger (>0.5 μm) particles, accounting for only 7.6% by number of the 300 °C across all sizes, suggesting this type are quite volatile. On the contrary, NaK–EC and Metal–EC showed an increasing contribution to the heated particles, particularly for the larger particles. This is due to their high non-volatility and reclassification of other particles as NaK–EC or Metal–EC after the volatilization of semi-volatile species. It is also possibly that larger particles shrank into the small size range with heating, resulting in higher number of Metal–EC and NaK–EC at 300 °C compared to ambient temperature. The contribution of ECOC particle type did not show significant shift with heating. Huffman et al. (2009) and Donahue et al. (2012) have shown the presence of significant less volatile organic mass fractions in biomass burning smoke, which is consistent with the non-volatility of organic species associated with ECOC particles in this study. In summary, NaK–EC was the major particle type at 0.2–0.3 μm at 300 °C. Correspondingly, the main particle types present from 0.4 to 0.5 μm were NaK–EC (47% by number) and ECOC (30%). At 1.2–1.3 μm, NaK–EC (49%) and Metal–EC (46%) were the dominant types. NaK–EC is the dominant EC particle type detected in the smoke of the coal combustion (Fig. S9). Metal–EC is likely to be produced by industrial high-temperature processes (Furutani et al., 2011; Zhang et al., 2014). Large amounts of metal-containing particles from anthropogenic sources have been detected in polluted air (Moffet et al., 2008).

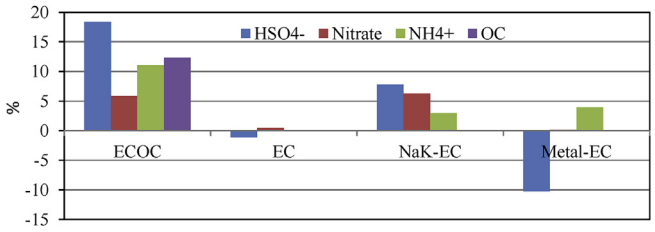

Fig. 5. Difference of fraction remaining for the selected ion markers (HSO_4^-, nitrate (NO_3^-/NO_2^-), NH_4^+, OC ($C_2H_3O^+$)) in each EC-containing particles type during hazy days and unpolluted days. Positive values suggest lower volatility during the hazy days, whereas negative values indicate the opposite results.

3.5. Atmospheric implication

The volatility and optical properties of EC particles are inextricably linked in the atmosphere. Photochemical aging leads to the presence of secondary components associated with EC. These non-absorbing and/or absorbing (brown carbon) coatings can lead to the absorption enhancement in principle via the absorbing shell and the lensing effect (Lack and Cappa, 2010). In this study, the volatility of secondary inorganic ions and brown carbon was shown to be variable dependent on particle types and atmospheric conditions, which are also observed in other studies (Cappa et al., 2012; Nakayama et al., 2014; Poulain et al., 2014). The different volatility of EC particle types will directly affect the optical properties by modifying the refractive index and the shell thickness (Cappa et al., 2012; Nakayama et al., 2014). Higher refractive index of coating material and thicker shell coating will result in more absorption enhancement (Pratt and Prather, 2009). A representative value of refractive index of anthropogenic SOA is around 1.55 (Kim and Paulson, 2013). The refractive indices of inorganic species are in a wide range from 1.3 to 2.5. The relationship between the volatility and refractive indices of coating material associated with different EC particles in China is still not well understood. This needs further more in-depth investigation.

4. Conclusions

Direct observation of real-time single particle volatility of EC-containing particles was performed by a thermodiluter coupled to a SPAMS during the spring of 2013 in the PRD region, China. Of the total unheated particles in this study, 53% of the unheated particles contained EC. Based on the dominant chemical species present in the mass spectra of individual particles, EC-containing particles were clustered into four types EC, OCEC, NaK–EC and Metal–EC. The results show that the volatility of EC-containing particles probably relied on the EC particle types and the molecular forms of secondary ions. Among the four types, the EC type was quite volatile. The loss of nitrate and sulfate associated with the EC-containing particles was in the form of ammonium salt. Meanwhile, the volatility of EC-containing particles decreased during the polluted hazy days. The volatility and optical properties of EC particles are inextricably linked in the atmosphere. Their relationship will be investigated in the further research.

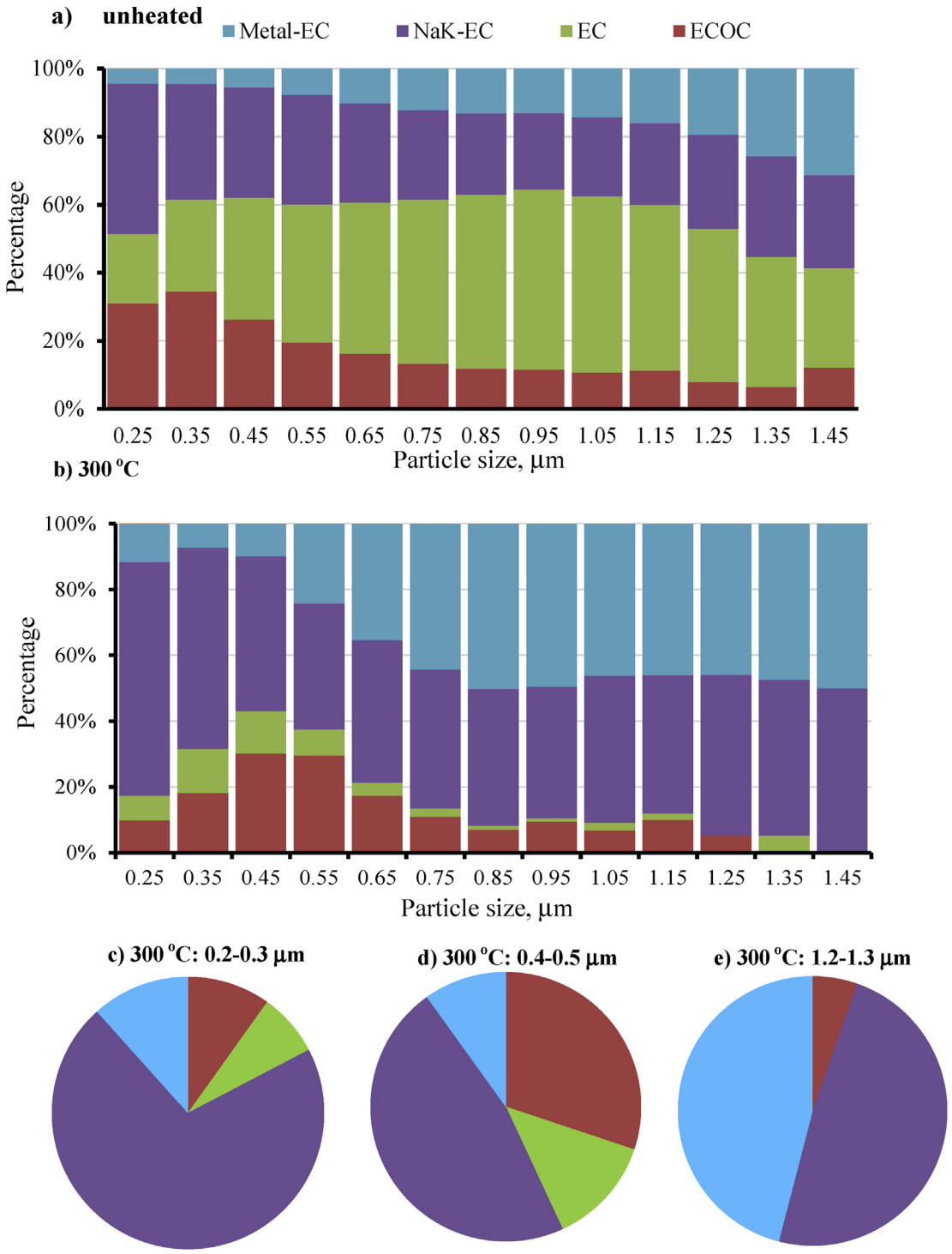

Fig. 6. Size-resolved chemical composition of (a) unheated and (b) 300 °C heated EC-containing particles. Relative fractions of 300 °C particle residues are illustrated for (c) 0.2–0.3 μm, (d) 0.7–0.8 μm, and (e) 1.2–1.3 μm.

Acknowledgments

This work was supported by " Strategic Priority Research Program (B) " of the Chinese Academy of Sciences(XDB05020205), National Natural Science Foundation of China (No. 41405131 and 41403091) and Foundation for Leading Talents from Guangdong Province Government. This is contribution from CASGIG No. IS-2108.

Appendix A. Supplementary data

Supplementary data related to this article can be found at http://dx.doi.org/10.1016/j.atmosenv.2015.08.012

References

Andreae, M.O., Gelencser, A., 2006. Black carbon or brown carbon? The nature of light-absorbing carbonaceous aerosols. Atmos. Chem. Phys. 6, 3131–3148.

Bi, X.H., Zhang, G.H., Li, L., Wang, X.M., Li, M., Sheng, G.Y., Fu, J.M., Zhou, Z., 2011. Mixing state of biomass burning particles by single particle aerosol mass spectrometer in the urban area of PRD, China. Atmos. Environ. 45, 3447–3453.
Bond, T.C., Doherty, S.J., Fahey, D.W., Forster, P.M., Berntsen, T., DeAngelo, B.J., Flanner, M.G., Ghan, S., Karcher, B., Koch, D., Kinne, S., Kondo, Y., Quinn, P.K., Sarofim, M.C., Schultz, M.G., Schulz, M., Venkataraman, C., Zhang, H., Zhang, S., Bellouin, N., Guttikunda, S.K., Hopke, P.K., Jacobson, M.Z., Kaiser, J.W., Klimont, Z., Lohmann, U., Schwarz, J.P., Shindell, D., Storelvmo, T., Warren, S.G., Zender, C.S., 2013. Bounding the role of black carbon in the climate system: a scientific assessment. J. Geophys. Res. Atmos. 118, 5380–5552.
Cappa, C.D., Onasch, T.B., Massoli, P., Worsnop, D.R., Bates, T.S., Cross, E.S., Davidovits, P., Hakala, J., Hayden, K.L., Jobson, B.T., Kolesar, K.R., Lack, D.A., Lerner, B.M., Li, S.M., Mellon, D., Nuaaman, I., Olfert, J.S., Petaja, T., Quinn, P.K., Song, C., Subramanian, R., Williams, E.J., Zaveri, R.A., 2012. Radiative absorption enhancements due to the mixing state of atmospheric black carbon. Science 337, 1078–1081.
Chhabra, P.S., Ng, N.L., Canagaratna, M.R., Corrigan, A.L., Russell, L.M., Worsnop, D.R., Flagan, R.C., Seinfeld, J.H., 2011. Elemental composition and oxidation of chamber organic aerosol. Atmos. Chem. Phys. 11, 8827–8845.
Clarke, A.D., Shinozuka, Y., Kapustin, V.N., Howell, S., Huebert, B., Doherty, S., Anderson, T., Covert, D., Anderson, J., Hua, X., Moore, K.G., McNaughton, C., Carmichael, G., Weber, R., 2004. Size distributions and mixtures of dust and black carbon aerosol in Asian outflow: physiochemistry and optical properties. J. Geophys. Res. Atmos. 109 (D15) http://dx.doi.org/10.1029/2003JD004378.
Dai, S.H., Bi, X.H., Huang, H., Zhang, G.H., He, J.J., Wu, G.C., Sheng, G.Y., Fu, J.M., Zhou, Z., 2014. Measurement of particle volatility using single particle aerosol mass spectrometry tandem thermodiluter. Chin. J. Anal. Chem. 42, 1155–1160.
Denkenberger, K.A., Moffet, R.C., Holecek, J.C., Rebotier, T.P., Prather, K.A., 2007. Real-time, single-particle measurements of oligomers in aged ambient aerosol particles. Environ. Sci. Technol. 41, 5439–5446.
Donahue, N.M., Kroll, J.H., Pandis, S.N., Robinson, A.L., 2012. A two-dimensional volatility basis set – part 2: diagnostics of organic-aerosol evolution. Atmos. Chem. Phys. 12, 615–634.
Engler, C., Rose, D., Wehner, B., Wiedensohler, A., Bruggemann, E., Gnauk, T., Spindler, G., Tuch, T., Birmili, W., 2007. Size distributions of non-volatile particle residuals (D-p < 800 nm) at a rural site in Germany and relation to air mass origin. Atmos. Chem. Phys. 7, 5785–5802.
Furutani, H., Jung, J.Y., Miura, K., Takami, A., Kato, S., Kajii, Y., Uematsu, M., 2011. Single-particle chemical characterization and source apportionment of iron-containing atmospheric aerosols in Asian outflow. J. Geophys. Res. Atmos. 116, D18204. http://dx.doi.org/10.1029/2011JD015867.
Ge, X.L., Zhang, Q., Sun, Y.L., Ruehl, C.R., Setyan, A., 2012. Effect of aqueous-phase processing on aerosol chemistry and size distributions in Fresno, California, during wintertime. Environ. Chem. 9, 221–235.
Hallquist, M., Wenger, J.C., Baltensperger, U., Rudich, Y., Simpson, D., Claeys, M., Dommen, J., Donahue, N.M., George, C., Goldstein, A.H., Hamilton, J.F., Herrmann, H., Hoffmann, T., Iinuma, Y., Jang, M., Jenkin, M.E., Jimenez, J.L., Kiendler-Scharr, A., Maenhaut, W., McFiggans, G., Mentel, T.F., Monod, A., Prevot, A.S.H., Seinfeld, J.H., Surratt, J.D., Szmigielski, R., Wildt, J., 2009. The formation, properties and impact of secondary organic aerosol: current and emerging issues. Atmos. Chem. Phys. 9, 5155–5236.
Hatch, L.E., Pratt, K.A., Huffman, J.A., Jimenez, J.L., Prather, K.A., 2014. Impacts of aerosol aging on laser desorption/ionization in single-particle mass spectrometers. Aerosol Sci. Technol. 48, 1050–1058.
He, Q.F., Ding, X., Wang, X.M., Yu, J.Z., Fu, X.X., Liu, T.Y., Zhang, Z., Xue, J., Chen, D.H., Zhong, L.J., Donahue, N.M., 2014. Organosulfates from pinene and isoprene over the Pearl River Delta, South China: seasonal variation and implication in formation mechanisms. Environ. Sci. Technol. 48, 9236–9245.
Heal, M.R., Kumar, P., Harrison, R.M., 2012. Particles, air quality, policy and health. Chem. Soc. Rev. 41, 6606–6630.
Huffman, J.A., Docherty, K.S., Mohr, C., Cubison, M.J., Ulbrich, I.M., Ziemann, P.J., Onasch, T.B., Jimenez, J.L., 2009. Chemically-resolved volatility measurements of organic aerosol from different sources. Environ. Sci. Technol. 43, 5351–5357.
Huffman, J.A., Ziemann, P.J., Jayne, J.T., Worsnop, D.R., Jimenez, J.L., 2008. Development and characterization of a fast-stepping/scanning thermodenuder for chemically-resolved aerosol volatility measurements. Aerosol Sci. Technol. 42, 395–407.
Jeong, C.H., McGuire, M.L., Godri, K.J., Slowik, J.G., Rehbein, P.J.G., Evans, G.J., 2011. Quantification of aerosol chemical composition using continuous single particle measurements. Atmos. Chem. Phys. 11, 7027–7044.
Jimenez, J.L., Canagaratna, M.R., Donahue, N.M., Prevot, A.S.H., Zhang, Q., Kroll, J.H., DeCarlo, P.F., Allan, J.D., Coe, H., Ng, N.L., Aiken, A.C., Docherty, K.S., Ulbrich, I.M., Grieshop, A.P., Robinson, A.L., Duplissy, J., Smith, J.D., Wilson, K.R., Lanz, V.A., Hueglin, C., Sun, Y.L., Tian, J., Laaksonen, A., Raatikainen, T., Rautiainen, J., Vaattovaara, P., Ehn, M., Kulmala, M., Tomlinson, J.M., Collins, D.R., Cubison, M.J., Dunlea, E.J., Huffman, J.A., Onasch, T.B., Alfarra, M.R., Williams, P.I., Bower, K., Kondo, Y., Schneider, J., Drewnick, F., Borrmann, S., Weimer, S., Demerjian, K., Salcedo, D., Cottrell, L., Griffin, R., Takami, A., Miyoshi, T., Hatakeyama, S., Shimono, A., Sun, J.Y., Zhang, Y.M., Dzepina, K., Kimmel, J.R., Sueper, D., Jayne, J.T., Herndon, S.C., Trimborn, A.M., Williams, L.R., Wood, E.C., Middlebrook, A.M., Kolb, C.E., Baltensperger, U., Worsnop, D.R., 2009. Evolution of organic aerosols in the atmosphere. Science 326, 1525–1529.
Johnson, G.R., Ristovski, Z., Morawska, L., 2004a. Application of the VH-TDMA technique to coastal ambient aerosols. Geophys. Res. Lett. 31.
Johnson, G.R., Ristovski, Z., Morawska, L., 2004b. Method for measuring the hygroscopic behaviour of lower volatility fractions in an internally mixed aerosol. J. Aerosol Sci. 35, 443–455.
Jonsson, A.M., Hallquist, M., Saathoff, H., 2007. Volatility of secondary organic aerosols from the ozone initiated oxidation of alpha-pinene and limonene. J. Aerosol Sci. 38, 843–852.
Kim, H., Paulson, S.E., 2013. Real refractive indices and volatility of secondary organic aerosol generated from photooxidation and ozonolysis of limonene, alpha-pinene and toluene. Atmos. Chem. Phys. 13, 7711–7723.
Knudsen, J.N., Jensen, P.A., Dam-Johansen, K., 2004. Transformation and release to the gas phase of Cl, K, and S during combustion of annual biomass. Energy Fuels 18, 1385–1399.
Kolb, C.E., Worsnop, D.R., 2012. Chemistry and composition of atmospheric aerosol particles. Annu. Rev. Phys. Chem. 63, 471–491.
Kostenidou, E., Lee, B.H., Engelhart, G.J., Pierce, J.R., Pandis, S.N., 2009. Mass spectra deconvolution of low, medium, and high volatility biogenic secondary organic aerosol. Environ. Sci. Technol. 43, 4884–4889.
Kroll, J.H., Seinfeld, J.H., 2008. Chemistry of secondary organic aerosol: formation and evolution of low-volatility organics in the atmosphere. Atmos. Environ. 42, 3593–3624.
Lack, D.A., Cappa, C.D., 2010. Impact of brown and clear carbon on light absorption enhancement, single scatter albedo and absorption wavelength dependence of black carbon. Atmos. Chem. Phys. 10, 4207–4220.
Lee, B.H., Pierce, J.R., Engelhart, G.J., Pandis, S.N., 2011. Volatility of secondary organic aerosol from the ozonolysis of monoterpenes. Atmos. Environ. 45, 2443–2452.
Levy, M.E., Zhang, R.Y., Zheng, J., Tan, H.B., Wang, Y., Molina, L.T., Takahama, S., Russell, L.M., Li, G.H., 2014. Measurements of submicron aerosols at the California–Mexico border during the Cal–Mex 2010 field campaign. Atmos. Environ. 88, 308–319.
Li, L., Huang, Z.X., Dong, J.G., Li, M., Gao, W., Nian, H.Q., Fu, Z., Zhang, G.H., Bi, X.H., Cheng, P., Zhou, Z., 2011. Real time bipolar time-of-flight mass spectrometer for analyzing single aerosol particles. Int. J. Mass Spectrom. 303, 118–124.
Liu, D.Y., Wenzel, R.J., Prather, K.A., 2003. Aerosol time-of-flight mass spectrometry during the Atlanta supersite experiment: 1. Measurements. J. Geophys. Res. Atmos. 108 (D7), 8426. http://dx.doi.org/10.1029/2001JD001562.
Moffet, R.C., Desyaterik, Y., Hopkins, R.J., Tivanski, A.V., Gilles, M.K., Wang, Y., Shutthanandan, V., Molina, L.T., Abraham, R.G., Johnson, K.S., Mugica, V., Molina, M.J., Laskin, A., Prather, K.A., 2008. Characterization of aerosols containing Zn, Pb, and Cl from an industrial region of Mexico City. Environ. Sci. Technol. 42, 7091–7097.
Moffet, R.C., Prather, K.A., 2009. In-situ measurements of the mixing state and optical properties of soot with implications for radiative forcing estimates. Proc. Natl. Acad. Sci. U. S. A. 106, 11872–11877.
Murphy, D.M., Thomson, D.S., 1997a. Chemical composition of single aerosol particles at Idaho Hill: negative ion measurements. J. Geophys. Res. Atmos. 102, 6353–6368.
Murphy, D.M., Thomson, D.S., 1997b. Chemical composition of single aerosol particles at Idaho Hill: positive ion measurements. J. Geophys. Res. Atmos. 102, 6341–6352.
Nakayama, T., Ikeda, Y., Sawada, Y., Setoguchi, Y., Ogawa, S., Kawana, K., Mochida, M., Ikemori, F., Matsumoto, K., Matsumi, Y., 2014. Properties of light-absorbing aerosols in the Nagoya urban area, Japan, in August 2011 and January 2012: contributions of brown carbon and lensing effect. J. Geophys. Res. Atmos. 119, 12721–12739.
Ng, N.L., Chhabra, P.S., Chan, A.W.H., Surratt, J.D., Kroll, J.H., Kwan, A.J., McCabe, D.C., Wennberg, P.O., Sorooshian, A., Murphy, S.M., Dalleska, N.F., Flagan, R.C., Seinfeld, J.H., 2007. Effect of NOx level on secondary organic aerosol (SOA) formation from the photooxidation of terpenes. Atmos. Chem. Phys. 7, 5159–5174.
Poulain, L., Birmili, W., Canonaco, F., Crippa, M., Wu, Z.J., Nordmann, S., Spindler, G., Prevot, A.S.H., Wiedensohler, A., Herrmann, H., 2014. Chemical mass balance of 300 degrees C non-volatile particles at the tropospheric research site Melpitz, Germany. Atmos. Chem. Phys. 14, 10145–10162.
Pratt, K.A., Murphy, S.M., Subramanian, R., DeMott, P.J., Kok, G.L., Campos, T., Rogers, D.C., Prenni, A.J., Heymsfield, A.J., Seinfeld, J.H., Prather, K.A., 2011. Flight-based chemical characterization of biomass burning aerosols within two prescribed burn smoke plumes. Atmos. Chem. Phys. 11, 12549–12565.
Pratt, K.A., Prather, K.A., 2009. Real-time, single-particle volatility, size, and chemical composition measurements of aged urban aerosols. Environ. Sci. Technol. 43, 8276–8282.
Qin, X.Y., Pratt, K.A., Shields, L.G., Toner, S.M., Prather, K.A., 2012. Seasonal comparisons of single-particle chemical mixing state in riverside, CA. Atmos. Environ. 59, 587–596.
Ramanathan, V., Carmichael, G., 2008. Global and regional climate changes due to black carbon. Nat. Geosci. 1, 221–227.
Ramanathan, V., Crutzen, P.J., Kiehl, J.T., Rosenfeld, D., 2001. Atmosphere – aerosols, climate, and the hydrological cycle. Science 294, 2119–2124.
Robinson, A.L., Donahue, N.M., Shrivastava, M.K., Weitkamp, E.A., Sage, A.M., Grieshop, A.P., Lane, T.E., Pierce, J.R., Pandis, S.N., 2007. Rethinking organic aerosols: semivolatile emissions and photochemical aging. Science 315, 1259–1262.
Romero, F., Oehme, M., 2005. Organosulfates – a new component of humic-like substances in atmospheric aerosols? J. Atmos. Chem. 52, 283–294.
Seinfeld, J.H., Pandis, S.N., 2006. From Air Pollution to Climate Change. John Wiley & Sons I, New Jersey.

Silva, P.J., Liu, D.Y., Noble, C.A., Prather, K.A., 1999. Size and chemical characterization of individual particles resulting from biomass burning of local Southern California species. Environ. Sci. Technol. 33, 3068–3076.

Song, X.H., Hopke, P.K., Fergenson, D.P., Prather, K.A., 1999. Classification of single particles analyzed by ATOFMS using an artificial neural network, ART-2A. Anal. Chem. 71, 860–865.

Wang, X.F., Gao, S., Yang, X., Chen, H., Chen, J.M., Zhuang, G.S., Surratt, J.D., Chan, M.N., Seinfeld, J.H., 2010. Evidence for high molecular weight nitrogen-containing organic salts in urban aerosols. Environ. Sci. Technol. 44, 4441–4446.

Wang, X.M., Ding, X., Fu, X.X., He, Q.F., Wang, S.Y., Bernard, F., Zhao, X.Y., Wu, D., 2012. Aerosol scattering coefficients and major chemical compositions of fine particles observed at a rural site hit the central Pearl River Delta, South China. J. Environ. Sci. China 24, 72–77.

Yadav, R., Saoud, K., Rasouli, F., Hajaligol, M., Fenner, R., 2004. Study of cigarette smoke aerosol using time of flight mass spectrometry. J. Anal. Appl. Pyrolysis 72, 17–25.

Zhang, G., Bi, X., Chan, L., Wang, X., Sheng, G., Fu, J., 2013a. Size-segregated chemical characteristics of aerosol during haze in an urban area of the Pearl River Delta region, China, urban climate, 2013. Urban Clim. 4, 74–84.

Zhang, G., Bi, X., Li, L., Chan, L.Y., Li, M., Wang, X., Sheng, G., Fu, J., Zhou, Z., 2013b. Mixing state of individual submicron carbon-containing particles during spring and fall seasons in urban Guangzhou, China: a case study. Atmos. Chem. Phys. 13, 4723–4735.

Zhang, G.H., Bi, X.H., Lou, S.R., Li, L., Wang, H.L., Wang, X.M., Zhou, Z., Sheng, G.Y., Fu, J.M., Chen, C.H., 2014. Source and mixing state of iron-containing particles in Shanghai by individual particle analysis. Chemosphere 95, 9–16.